Low-temperature and high-temperature approximations for penetrable-sphere fluids: Comparison with Monte Carlo simulations and integral equation theories

Alexandr Malijevský[*]

E. Hála Laboratory of Thermodynamics, Academy of Science of the Czech Republic, Prague 6, Czech Republic
and Institute of Theoretical Physics, Faculty of Mathematics and Physics, Charles University, Prague 8, Czech Republic

Santos B. Yuste[†] and Andrés Santos[‡]

Departamento de Física, Universidad de Extremadura, E-06071 Badajoz, Spain

The two-body interaction in dilute solutions of polymer chains in good solvents can be modeled by means of effective bounded potentials, the simplest of which being that of penetrable spheres (PSs). In this paper we construct two simple analytical theories for the structural properties of PS fluids: a low-temperature (LT) approximation, that can be seen as an extension to PSs of the well-known solution of the Percus-Yevick (PY) equation for hard spheres, and a high-temperature (HT) approximation based on the exact asymptotic behavior in the limit of infinite temperature. Monte Carlo simulations for a wide range of temperatures and densities are performed to assess the validity of both theories. It is found that, despite their simplicity, the HT and LT approximations exhibit a fair agreement with the simulation data within their respective domains of applicability, so that they complement each other. A comparison with numerical solutions of the PY and the hypernetted-chain approximations is also carried out, the latter showing a very good performance, except inside the core at low temperatures.

I. INTRODUCTION

Since Wertheim and Thiele's analytical solution [1] of the Percus–Yevick (PY) integral equation for hard spheres (HSs), a great deal of effort has been devoted to (approximately) describe the equilibrium behavior of simple liquids. Potentials capturing short-range harsh repulsion (with or without an attractive contribution) have deserved particular interest. Recently, the mainstream of attention has been transferred to more complex liquids, such as colloidal dispersions. Interestingly enough, coarse-graining techniques reveal that apparently toy interaction models, some of them not diverging at zero separation, can serve as excellent effective potentials in soft condensed matter.

While the effective interaction between two sterically stabilized colloidal particles can be accurately modeled by the HS potential [2], the effective two-body interaction in other colloidal systems can be much softer. For instance, the interaction potential for star polymers in good solvents diverges only logarithmically for short distances [2,3]. In the case of dilute solutions of polymer chains in good solvents, the distance between the centers of mass of two chains can be smaller than the sum of their respective radii of gyration [2], so that the effective two-body potential is bounded. This implies the possibility of particles to form clusters, which makes the problem greatly nontrivial. A simple class of bounded potentials is described by the purely repulsive generalized exponential model [4–6] parametrized by an index n. In the particular case $n=2$ one recovers the Gaussian core

model, which has been widely studied [7–14]. This model exhibits re-entrant melting [11] and the same is expected if $n<2$ [4,5]. On the other hand, a clustering transition, which has been analyzed in detail for $n=4$ [5,6], is predicted if $n>2$ [4,5,11]. In the limit $n \rightarrow \infty$, the generalized exponential model reduces to the penetrable-sphere (PS) model

$$\varphi(r) = \begin{cases} \epsilon, & r < \sigma, \\ 0, & r > \sigma. \end{cases} \quad (1.1)$$

This model has been extensively investigated from different perspectives [11,15–30]. Density-functional theory [19,20] predicts a freezing transition to fcc solid phases with multiply occupied lattice sites. The existence of clusters of overlapped particles (or "clumps") in the PS crystal and glass was already pointed out by Klein *et al.* [18], who also performed Monte Carlo (MC) simulations on the system. In the fluid phase, the standard integral equation theories are not reliable in describing the structure of the PS fluid inside the core at low temperatures [19,21]: the number of overlapped pairs is overestimated by the hypernetted-chain (HNC) theory, while it is strongly underestimated by the PY theory. Other more sophisticated closures [21,25], as well as Rosenfeld's fundamental-measure theory [22], are able to predict the correlations functions with a higher precision.

In any case, the classical theories (PY and HNC), as well as the alternative ones [21,22,25], require numerical work to get the correlation functions, such as the radial distribution function $g(r)$ or, equivalently, the cavity (or background) function $y(r) \equiv e^{\varphi(r)/k_B T} g(r)$, where k_B is the Boltzmann constant and T is the temperature.

In general, the functions $g(r)$ and $y(r)$ convey the same physical information. However, the cavity function $y(r)$ is a much more regular function than the radial distribution func-

---
*malijevsky@icpf.cas.cz
†santos@unex.es; URL: http://www.unex.es/eweb/fisteor/santos/
‡andres@unex.es; URL: http://www.unex.es/eweb/fisteor/andres/

tion $g(r)$. In particular, if the interaction potential $\varphi(r)$ diverges in a certain region (as happens for HSs with $r < \sigma$), $g(r)$ vanishes in that region, while $y(r)$ keeps being well defined. In that case, $y(r)$ provides more physical information than $g(r)$. In this context, it is worth recalling the physical interpretation of $y(r)$ as being proportional to the probability of accepting the insertion of an additional test particle at a distance r from a given particle with which the test particle is assumed not to interact [31].

Even in the one-dimensional (1D) case, the PS model is far from trivial, since interactions are not restricted to nearest neighbors and so its exact solution is not known [29]. Useful information, however, can be obtained in analytical or semi-analytical form in some limiting cases. Thus in the combined high-temperature and high-density limit the PS model is amenable to an exact analytical treatment for any number of dimensions [26]. An interesting consequence of the boundedness of the PS potential in the one-dimensional (1D) case is the plausible existence of a fluid-crystal phase transition [26], thus providing one of the rare examples of phase transitions in 1D systems [32]. In the complementary low-density domain, the cavity function $y(r)$ has been recently determined to second order in density at any temperature [30]. Comparison of the second-order contribution to $y(r)$ with the corresponding PY and HNC predictions shows that both are rather poor inside the core for low and moderate temperatures (say $T^* \equiv k_B T / \epsilon \lesssim 1$) but the HNC theory rapidly improves as the temperature increases. Finally, at zero temperature ($T^* \to 0$), the PS model becomes identical with the HS model. Although the correlation functions of HSs are not exactly known (except in the 1D case), the PY theory is analytically solvable for that interaction model [1], the corresponding radial distribution function exhibiting a general good agreement with computer simulations [33,34]. However, this good agreement of the PY $g(r)$ for HSs can be misleading. As mentioned before, $g(r)$ vanishes inside the core ($r < \sigma$) for HSs but the cavity function $y(r)$ does not. It turns out that the PY $y(r)$ for HSs is much worse for $r < \sigma$ than for $r > \sigma$ (even in the 1D case [29]), this deficiency being inherited by the PY solution for PSs [30], in which case $g(r) \neq 0$ for $r < \sigma$.

The main aim of this work is to construct two simple analytical theories for the structural properties of the three-dimensional PS fluid. One of them is based on the exact solution of the PY equation for HSs, modified inside the core. Since, as noted above, the HS fluid is the zero-temperature limit of the PS fluid, this extension of the PY solution is expected to be adequate for low and moderate temperatures and so we will refer to it as the low-temperature (LT) theory. The other approach, here referred to as the high-temperature (HT) theory, is a simple extension to finite temperatures of the exact asymptotic correlation functions in the limit $T^* \to \infty$. Both approximations are compared with our own MC simulations as well as with numerical solutions of the PY and HNC integral equations. It is observed that the LT and HT theories complement each other quite well, exhibiting a good agreement with the simulation data in their respective domains of applicability, which are wider than what one might have anticipated. It is also found that the

HNC theory has an excellent behavior, except inside the core at low temperatures, while the PY results are always very poor inside the core.

In the next section some basic properties of the PS fluid are presented. Next, the zero-temperature limit is considered in Sec. III, where special attention is paid to the PY solution for HSs and an improved modified version of it in the overlapping region is proposed. Our LT and HT theories are worked out in Secs. IV and V, respectively. Section VI shows the comparison with MC simulation data and with the PY and HNC results for a wide range of representative states. Finally, the paper is closed in Sec. VII with a summary and discussion of the results.

II. THE PS MODEL: SOME BASIC RESULTS

Let us consider a three-dimensional fluid made of particles interacting via the pairwise PS potential (1.1). The cavity function $y(r) \equiv e^{\varphi(r)/k_B T} g(r)$ is a continuous function of r, while the discontinuity of the potential at $r = \sigma$ is transferred to the radial distribution function $g(r)$:

$$g(r) = y(r) - xy(r)\Theta(1-r), \qquad (2.1)$$

where

$$x \equiv 1 - e^{-1/T^*} \qquad (2.2)$$

is a temperature-dependent parameter bounded between $x = 0$ ($T^* \to \infty$) and $x = 1$ ($T^* = 0$), $\Theta(z)$ is the Heaviside step function, and henceforth the distance is measured in units of σ. The parameter x represents the probability of rejecting an overlap of two particles in an MC move. Some properties of the Laplace transform $G(t)$ of $rg(r)$ are presented in Appendix A.

In the limit of infinitely high temperatures at finite densities the height of the potential barrier becomes negligible and so the system behaves as an ideal gas. Apart from this trivial situation, the exact form of $y(r)$ is not known, except (a) to second order in density for any temperature [30] and (b) in the high-temperature and high-density limit [26].

A. Low-density limit

To first order in density, the cavity function is exactly given by

$$y(r) = 1 + \frac{1}{2}\eta x^2 (2-r)^2 (r+4)\Theta(2-r) + \mathcal{O}(\eta^2), \quad (2.3)$$

where $\eta \equiv (\pi/6)\rho\sigma^3$, ρ being the number density. In the case of HSs, η represents the packing fraction and so here we will retain that name (although in the PS model there is no *a priori* upper bound for it). From Eq. (2.3) one can easily get

$$y(1) = 1 + \frac{5}{2}\eta x^2 + \mathcal{O}(\eta^2), \quad y'(1) = -\frac{9}{2}\eta x^2 + \mathcal{O}(\eta^2),$$

$$(2.4)$$

$$y(0) = 1 + 8\eta x^2 + \mathcal{O}(\eta^2), \quad y'(0) = -6\eta x^2 + \mathcal{O}(\eta^2),$$
$$(2.5)$$

where the prime denotes a derivative with respect to r. The second-order contribution in the density expansion (2.3) is also known [30], but it will not be needed here.

B. High-temperature limit

In the high-temperature and high-density limit ($T^* \to \infty$, $\eta \to \infty$, $\eta x = \text{const}$), the cavity function has the form [26]

$$y(r) = 1 + xw(r) + \mathcal{O}(x^2), \quad (2.6)$$

where $w(r)$ is the inverse Fourier transform of

$$\widetilde{w}(k) = \frac{96\pi\eta x(k\cos k - \sin k)^2}{k^3[k^3 - 24\eta x(k\cos k - \sin k)]}. \quad (2.7)$$

The virial expansion of the function $w(r)$ is worked out in Appendix B, where it is shown that the series converges for $\eta x < \frac{1}{8}$. It is also proven in Appendix B that $w(r)$ has a fourth-order discontinuity at $r = 1$ and a discontinuity of order $2(n-1)$ at $r = n \geq 2$.

The denominator in Eq. (2.7) has a real root if $\eta x \geq \hat{\eta}_0 \simeq 1.45$. This indicates the existence of a spinodal transition (Kirkwood's instability) in the high-temperature limit as $\eta x \to \hat{\eta}_0$ from below. This instability is preempted by the freezing transition, which can be estimated to occur at $\eta x \approx 0.6$ [26].

III. ZERO-TEMPERATURE LIMIT

A. Cavity function inside the core

In the limit of zero temperature ($T^* \to 0$) the penetrable particles become impenetrable, i.e., they become HSs. Therefore in that limit the radial distribution function $g(r)$ vanishes inside the core ($r < 1$). However, the cavity function is still well defined in that region. In connection with this point, it might be useful to recall two zero-separation theorems for HS fluids [35]:

$$\ln y(0) = \frac{1}{k_B T}\mu_{\text{ex}} = Z(\rho) - 1 + \int_0^\rho d\rho' \frac{Z(\rho') - 1}{\rho'}, \quad (3.1)$$

$$\frac{y'(0)}{y(0)} = -6\eta y(1). \quad (3.2)$$

In Eq. (3.1), μ_{ex} is the HS excess chemical potential and $Z = 1 + 4\eta y(1)$ is the HS compressibility factor.

It is interesting to see how the cavity function for PSs converges to that of HSs as the temperature decreases. Figure 1 compares our MC simulation data obtained for PSs [36] at $T^* = 0.2$ ($1-x \simeq 7 \times 10^{-3}$), $T^* = 0.13$ ($1-x \simeq 5 \times 10^{-4}$), and $T^* = 0.1$ ($1-x \simeq 5 \times 10^{-5}$) with the MC results obtained by Labík and Malijevský for HSs [31]. Our PS data were obtained by measuring $g(r)$ directly and then obtaining $y(r)$ inside the core as $y(r) = g(r)/(1-x)$. In contrast, the HS data of Ref. [31] were obtained by a particle-insertion method.
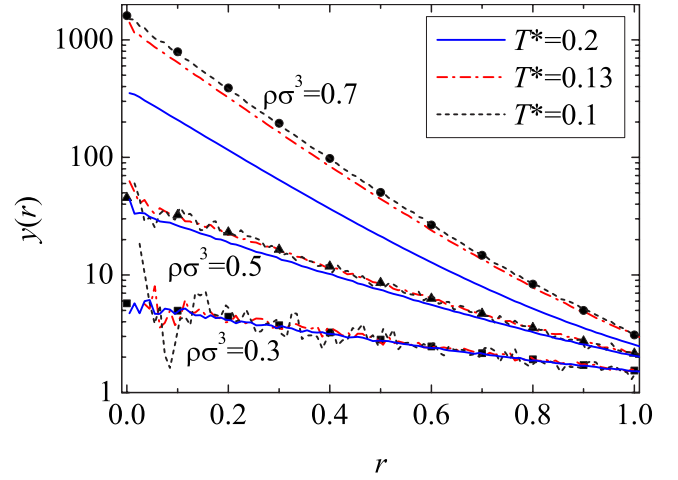

FIG. 1. (Color online) Plot of the cavity function $y(r)$ inside the core ($r < 1$) for densities $\rho\sigma^3 = 0.3$, $\rho\sigma^3 = 0.5$, and $\rho\sigma^3 = 0.7$. The symbols are MC simulation data for HSs [31]. The lines are our MC data for PSs at $T^* = 0.2$ (solid lines), $T^* = 0.13$ (dashed-dotted lines), and $T^* = 0.1$ (dashed lines).

We observe that for a density $\rho\sigma^3 = 0.3$ a temperature $T^* = 0.2$ is low enough to get results practically indistinguishable from those of HSs ($T^* = 0$). However, as the density increases one needs to keep lowering the temperature to get a good collapse. Thus for $\rho\sigma^3 = 0.5$ and $\rho\sigma^3 = 0.7$ the HS curves are recovered at $T^* = 0.13$ and $T^* = 0.1$, respectively. It is interesting to note that, although at $T^* = 0.2$ the probability of accepting an attempted overlap between two PSs is only $1 - x \simeq 7 \times 10^{-3}$, a density $\rho = 0.7$ is high enough to make the corresponding cavity function deviate strongly from that of HSs. Figure 1 also shows that at low densities and temperatures (e.g., $\rho\sigma^3 = 0.3$ and $T^* = 0.1$) the number of overlaps is very small and so the measured $y(r)$ presents large statistical fluctuations.

B. PY solution for HSs

It is well known that the radial distribution function $g(r)$ for HSs is rather well represented by the PY solution [1,33,34]. In that solution the auxiliary function $P(t)$ defined by Eq. (A5) has the explicit rational form

$$P(t) = -e^{-t}\frac{1 + L_1 t}{1 + S_1 t + S_2 t^2 + S_3 t^3}, \quad (3.3)$$

where the coefficients can be univocally determined by application of Eq. (A6). This yields [37,38]

$$L_1 = \frac{1 + \eta/2}{1 + 2\eta}, \quad (3.4)$$

$$S_1 = L_1 - 1, \quad (3.5)$$

$$S_2 = \frac{1}{2} - L_1, \quad (3.6)$$

$$S_3 = \frac{6\eta L_1 - 1 - 2\eta}{12\eta}. \quad (3.7)$$

Insertion of Eq. (3.3) into Eq. (A5) gives the Laplace transform $G(t)$ for HSs. It can be expressed as

$$G(t) = \sum_{n=1}^{\infty} F_n(t)e^{-nt}, \tag{3.8}$$

where

$$F_n(t) \equiv -\frac{t}{12\eta}\left(\frac{1+L_1 t}{1+S_1 t + S_2 t^2 + S_3 t^3}\right)^n. \tag{3.9}$$

The inverse Laplace transform of Eq. (3.8) yields

$$g(r) = \frac{1}{r}\sum_{n=1}^{\infty} f_n(r-n)\Theta(r-n), \tag{3.10}$$

where $f_n(r)$ is the inverse Laplace transform of $F_n(t)$. In particular,

$$y_{PY}(1) = \frac{1+\eta/2}{(1-\eta)^2}, \quad y'_{PY}(1) = -\frac{9\eta(1+\eta)}{2(1-\eta)^3}, \tag{3.11}$$

where henceforth we use the label PY in subscripts or superscripts to indicate explicit results derived from the PY solution for HSs. The contact value $y_{PY}(1)$ yields the virial route to the equation of state and from it one gets

$$\frac{1}{k_B T}\mu_{ex}^{PY} = 2\ln(1-\eta) + \frac{2\eta(5-2\eta)}{(1-\eta)^2}. \tag{3.12}$$

Equation (3.10) gives reasonable predictions for the HS radial distribution function [33,34]. However, the cavity function in the region $r<1$, which is given by

$$y_{PY}(r) = \frac{1}{(1-\eta)^4}\left((1+2\eta)^2 - 6\eta(1+\eta/2)^2 r \right.$$
$$\left. + \frac{\eta}{2}(1+2\eta)^2 r^3\right), \tag{3.13}$$

strongly underestimates the correct values, even to second order in density [30]. From Eq. (3.13) one gets

$$y_{PY}(0) = \frac{(1+2\eta)^2}{(1-\eta)^4}, \quad \frac{y'_{PY}(0)}{y_{PY}(0)} = -6\eta\left(\frac{1+\eta/2}{1+2\eta}\right)^2. \tag{3.14}$$

Equations (3.11), (3.12), and (3.14) are not consistent with the zero-separation theorems (3.1) and (3.2). In fact, the values of $y(0)$ and $y'(0)$ thermodynamically consistent with $y_{PY}(1)$ are

$$y_{mPY}(0) = (1-\eta)^2 \exp\left[\frac{2\eta(5-2\eta)}{(1-\eta)^2}\right], \tag{3.15}$$

$$\frac{y'_{mPY}(0)}{y_{mPY}(0)} = -6\eta\frac{1+\eta/2}{(1-\eta)^2}, \tag{3.16}$$

where here the label mPY stands for "modified" PY values. One can then modify the PY expression of $y(r)$ for $0 \le r \le 1$ as
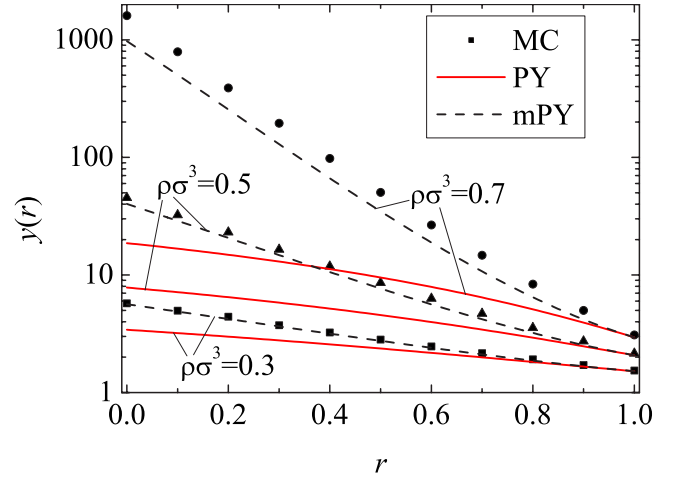

FIG. 2. (Color online) Plot of the HS cavity function $y(r)$ inside the core ($r<1$) for densities $\rho\sigma^3=0.3$ (squares), $\rho\sigma^3=0.5$ (triangles), and $\rho\sigma^3=0.7$ (circles). The symbols are MC simulation data [31], the solid lines are the PY predictions, Eq. (3.13), and the dashed lines are the modified PY predictions, Eq. (3.17).

$$y_{mPY}(r) = y_{PY}(r)e^{(r-1)^2(\lambda_0+\lambda_1 r)}, \tag{3.17}$$

where $y_{mPY}(1)=y_{PY}(1)$, $y'_{mPY}(1)=y'_{PY}(1)$, and the coefficients λ_0 and λ_1 are determined by imposing consistency with Eqs. (3.15) and (3.16), namely

$$\lambda_0 = \ln\frac{y_{mPY}(0)}{y_{PY}(0)}, \quad \lambda_1 = 2\lambda_0 + \frac{y'_{mPY}(0)}{y_{mPY}(0)} - \frac{y'_{PY}(0)}{y_{PY}(0)}. \tag{3.18}$$

Of course, the modified form (3.17) is not the only possible one that can be proposed to satisfy the zero-separation theorems with $y_{mPY}(1)=y_{PY}(1)$ and $y'_{mPY}(1)=y'_{PY}(1)$. The rationale behind Eq. (3.17) is that, since the HS cavity function grows so rapidly inside the core (see Fig. 1), it is convenient to add a polynomial correction to $\ln y_{PY}(r)$ rather than to $y_{PY}(r)$.

Figure 2 compares Eqs. (3.13) and (3.17) with MC data [31]. It is quite apparent that the PY is very inaccurate in the region $0 \le r \le 1$. However, the simple modified form (3.17), apart from incorporating the values of $y(0)$ and $y'(0)$ consistent with the PY contact value $y_{PY}(1)$ via the zero-separation theorems, is quite satisfactory. On the other hand, $y_{mPY}(r)$ underestimates the true values, this effect being especially visible at $\rho\sigma^3=0.7$. This is a consequence of the fact that, as is well known, $y_{PY}(1)$ is lower than the true contact value and this is transferred to $y_{mPY}(0)$ through Eq. (3.1).

In order to extend Eq. (3.15) to the PS case in Sec. IV, it is convenient to express $y_{mPY}(0)$ in terms of $y_{PY}(1)$. To that end, we first rewrite Eq. (3.15) in the form

$$y_{mPY}(0) = y_{PY}(1)e^{\alpha(\eta)\eta y_{PY}(1)}, \tag{3.19}$$

where

$$\alpha(\eta) \equiv \frac{1}{1 + \eta/2}\left[2(5 - 2\eta) + \frac{(1-\eta)^2}{\eta}\ln\frac{(1-\eta)^4}{1+\eta/2}\right].$$
(3.20)

It turns out that $\alpha(\eta)$ depends very weakly on η, deviating from $\alpha(0) = \frac{11}{2}$ less than 5% for $\eta < 0.48$. Therefore from a practical point of view we can approximate Eqs. (3.15) or (3.19) by

$$y_{\text{mPY}}(0) \simeq y_{\text{PY}}(1)e^{(11/2)\eta_{\text{PY}}(1)}.$$
(3.21)

In fact, we have checked that Eqs. (3.17) and (3.18), when implemented with Eq. (3.21) instead of Eq. (3.15), provides curves indistinguishable from the mPY curves plotted in Fig. 2, except at the density $\rho\sigma^3 = 0.7$, where Eq. (3.21) gives slightly better results.

IV. THE LOW-TEMPERATURE (LT) APPROXIMATION

Now we want to generalize to PSs the PY solution for HSs described in Sec. III, plus the modification (3.17) for $r < 1$, so that effects due to finite (but low) temperatures are incorporated. The resulting approximation for $g(r)$ will be essentially analytical, will reduce to the PY solution in the limit $T^* \to 0$, and will be better than the numerical solution of the genuine PY integral equation for PS model, except at high temperatures.

The steps are similar to the ones followed in the 1D case [29]. In a first stage, we keep the relationship (A5) between the Laplace transform $G(t)$ and the auxiliary function $P(t)$ and propose an explicit form for the latter. In a second stage, we modify the function $g(r)$ in the overlapping region in order to satisfy approximate extensions of the zero-separation theorems.

A. First stage

Our proposal for the function $P(t)$ defined by Eq. (A5) is

$$P(t) = \frac{L_0 - 1 - e^{-t}(L_0 + L_1 t)}{1 + S_1 t + S_2 t^2 + S_3 t^3},$$
(4.1)

which reduces to the PY form (3.3) for HSs if $L_0 = 1$. However, the presence of $L_0 \neq 1$ for $T^* \neq 0$ (i.e., $x \neq 1$) is necessary to satisfy the exact physical requirement (A7). Condition (A6) allows one to express the coefficients L_1, S_1, S_2, and S_3 in terms of L_0:

$$L_1 = L_0\frac{1 + \eta/2}{1 + 2\eta},$$
(4.2)

$$S_1 = L_1 - L_0,$$
(4.3)

$$S_2 = \frac{1}{2}L_0 - L_1,$$
(4.4)

$$S_3 = \frac{6\eta L_1 - 1 - 2\eta L_0}{12\eta}.$$
(4.5)

Inserting Eq. (4.1) into Eq. (A5) and expanding in powers of e^{-t}, one gets

$$G(t) = \sum_{n=0}^{\infty} F_n(t)e^{-nt},$$
(4.6)

where

$$F_0(t) = \frac{t}{12\eta}\frac{L_0 - 1}{L_0 + S_1 t + S_2 t^2 + S_3 t^3},$$
(4.7)

$$F_n(t) = -\frac{t}{12\eta}\frac{(1 + S_1 t + S_2 t^2 + S_3 t^3)(L_0 + L_1 t)^n}{(L_0 + S_1 t + S_2 t^2 + S_3 t^3)^{n+1}}, \quad n \geq 1.$$
(4.8)

Therefore

$$g(r) = \frac{1}{r}\sum_{n=0}^{\infty} f_n(r - n)\Theta(r - n),$$
(4.9)

where $f_n(r)$ is the inverse Laplace transform of $F_n(t)$. Equations (4.6) and (4.9) are formally analogous to Eqs. (3.8) and (3.10), respectively. However, some important differences can be observed: Eqs. (4.6) and (4.9) include extra contributions associated with $n=0$, Eq. (4.8) differs from Eq. (3.9), and Eqs. (4.2)–(4.5) differ from Eqs. (3.4)–(3.7). Obviously, Eqs. (4.2)–(4.9) reduce to Eqs. (3.4)–(3.10) if $L_0 = 1$. Since $L_0 \neq 1$ for PSs, the basic difference with respect to the HS case is that now one has $g(r) = f_0(r)/r \neq 0$ for $r < 1$. More specifically, application of the residue theorem to get the inverse Laplace transform of Eq. (4.7) yields

$$f_0(r) = \frac{1}{12\eta}\sum_{i=1}^{3} z_i\frac{L_0 - 1}{S_1 + 2S_2 z_i + 3S_3 z_i^2}e^{z_i r},$$
(4.10)

where z_i $(i=1,2,3)$ are the three roots of the cubic equation $L_0 + S_1 t + S_2 t^2 + S_3 t^3 = 0$. In particular,

$$f_0(1) = \frac{1}{12\eta}\sum_{i=1}^{3} z_i\frac{L_0 - 1}{S_1 + 2S_2 z_i + 3S_3 z_i^2}e^{z_i},$$
(4.11)

$$f_0'(1) = \frac{1}{12\eta}\sum_{i=1}^{3} z_i^2\frac{L_0 - 1}{S_1 + 2S_2 z_i + 3S_3 z_i^2}e^{z_i}.$$
(4.12)

One could also evaluate $f_0(0)$ and $f_0'(0)$ from Eq. (4.10), but it is easier to do it by a simpler alternative route. Taking into account the expansion of $F_0(t)$ for large t,

$$F_0(t) = \frac{L_0 - 1}{S_3}\frac{t^{-2}}{12\eta}\left(1 - \frac{S_2}{S_3}t^{-1}\right) + \mathcal{O}(t^{-4}),$$
(4.13)

one gets

$$f_0(r) = \frac{L_0 - 1}{S_3}\frac{r}{12\eta}\left(1 - \frac{S_2}{2S_3}r\right) + \mathcal{O}(r^3).$$
(4.14)

Therefore

$$f_0(0) = 0, \quad f_0'(0) = \frac{L_0 - 1}{12\eta S_3}. \tag{4.15}$$

Similarly,

$$F_1(t) = -\frac{L_1}{S_3} \frac{t^{-1}}{12\eta} \left[1 + \left(\frac{L_0}{L_1} - \frac{S_2}{S_3} \right) t^{-1} \right] + \mathcal{O}(t^{-3}), \tag{4.16}$$

so that

$$f_1(r) = -\frac{L_1}{S_3} \frac{1}{12\eta} \left[1 + \left(\frac{L_0}{L_1} - \frac{S_2}{S_3} \right) r \right] + \mathcal{O}(r^2), \tag{4.17}$$

$$f_1(0) = -\frac{L_1}{12\eta S_3}, \quad f_1'(0) = -\frac{L_0 - L_1 S_2/S_3}{12\eta S_3}. \tag{4.18}$$

So far, the parameter L_0 remains undetermined. We now fix it by imposing the continuity of the cavity function at $r = 1$, i.e., $y(1^-) = y(1^+)$. From Eq. (4.9) one has

$$ry(r) = \begin{cases} (1-x)^{-1} f_0(r), & 0 \le r \le 1, \\ f_0(r) + f_1(r-1), & 1 \le r \le 2. \end{cases} \tag{4.19}$$

Therefore

$$y(1^-) = \frac{1}{1-x} f_0(1), \quad y(1^+) = f_0(1) + f_1(0). \tag{4.20}$$

The condition $y(1^-) = y(1^+)$ yields

$$x f_0(1) = (1-x) f_1(0). \tag{4.21}$$

Insertion of Eqs. (4.11) and (4.18) into Eq. (4.21), together with Eqs. (4.2)–(4.5), renders a closed transcendental equation that gives L_0 as a function of x and η. This closes the proposal (4.9). In the zero-temperature limit ($x \to 1$), Eq. (4.21) becomes $f_0(1) = 0$, whose solution is simply $L_0 = 1$ and then we recover the analytical PY solution for HSs.

While Eq. (4.21) satisfies the condition $y(1^-) = y(1^+)$, it does not verify $y'(1^-) = y'(1^+)$, except at $T^* = 0$. In addition, it inherits from the PY solution for HSs a poor performance in the overlapping region, even at low temperatures. Both deficiencies are remedied by the next stage.

B. Second stage

In parallel with what we did in Sec. III in the case of the PY solution for HSs [cf. Eq. (3.17)], we propose now in the case of PSs an improved version of the approximation (4.9) in which only the radial distribution function in the overlapping region is modified, namely

$$g(r) = \frac{e^{Q(r)\Theta(1-r)}}{r} \sum_{n=0}^{\infty} f_n(r-n)\Theta(r-n), \tag{4.22}$$

where $Q(r)$ is a third-degree polynomial with the constraint $Q(1) = 0$ to maintain the continuity of $y(r)$ at $r = 1$ obtained in the first stage. The degree of $Q(r)$ is suggested by the structure of the exact cavity function to first order in density, Eq. (2.3), and by the polynomial appearing in the exponential of Eq. (3.17). Thus $Q(r)$ can be written as

$$Q(r) = (r-1)[A + B(r+2)(r-1) + Cr(r-1)]. \tag{4.23}$$

The parameters A, B, and C will be determined by imposing the continuity condition $y'(1^-) = y'(1^+)$, as well as approximate expressions for the zero-separation values $y(0)$ and $y'(0)$. According to Eq. (4.22), Eq. (4.19) is replaced by

$$ry(r) = \begin{cases} (1-x)^{-1} f_0(r) e^{Q(r)}, & 0 \le r \le 1, \\ f_0(r) + f_1(r-1), & 1 \le r \le 2. \end{cases} \tag{4.24}$$

The condition $y'(1^-) = y'(1^+)$ yields

$$A = \frac{x}{f_1(0)} \left[f_1'(0) - \frac{x}{1-x} f_0'(1) \right], \tag{4.25}$$

where use has been made of Eq. (4.21) and $f_0'(1)$, $f_1(0)$, and $f_1'(0)$ are given by Eqs. (4.12) and (4.18). It remains to determine the coefficients B and C. To that end, note that Eq. (4.24) implies

$$y(0) = \frac{e^{2B-A}}{1-x} \frac{L_0 - 1}{12\eta S_3}, \tag{4.26}$$

$$\frac{y'(0)}{y(0)} = A + C - 3B - \frac{S_2}{2S_3}, \tag{4.27}$$

where use has been made of Eq. (4.14). Therefore B and C can be expressed in terms of $y(0)$ and $y'(0)$ as follows:

$$B = \frac{1}{2}A + \frac{1}{2} \ln \left[(1-x) 12\eta \frac{S_3}{L_0 - 1} y(0) \right], \tag{4.28}$$

$$C = \frac{y'(0)}{y(0)} - A + 3B + \frac{S_2}{2S_3}. \tag{4.29}$$

To close the problem we need to propose approximate expressions for $y(0)$ and $y'(0)$. Here we take

$$\ln y(0) = \frac{11}{2} \eta x^5 y(1) + \ln \left[y(1) + \frac{11}{2} \eta(x^2 - x^5) y^2(1) \right], \tag{4.30}$$

$$\frac{y'(0)}{y(0)} = -6\eta x^2 y(1). \tag{4.31}$$

Equations (4.30) and (4.31) are exact to first order in density, as can be seen from Eqs. (2.4) and (2.5). In addition, Eqs. (4.30) and (4.31) reduce to Eqs. (3.21) and (3.2), respectively, in the zero-temperature limit ($x \to 1$). From that point of view, Eqs. (4.30) and (4.31) can be viewed as approximate extensions to $x \ne 1$ of the zero-separation theorems. A similar extension was proposed in the 1D case [29].

To check the reliability of Eqs. (4.30) and (4.31), we have tested them against MC simulations for a wide range of temperatures and densities. The results are displayed in Table I. It can be seen that Eqs. (4.30) and (4.31) compare reasonably well with simulations for all the states considered.

This closes the construction of our low-temperature (LT) approximation. In summary, for any desired density and tem-

TABLE I. MC simulation data for $y(1)$, $\ln y(0)$, and $y'(0)/y(0)$. The values obtained from the approximations (4.30) and (4.31) with the empirical $y(1)$ are also included.

T^*	η	$y(1)$	$\ln y(0)$	Eq. (4.30)	$-y'(0)/y(0)$	Eq. (4.31)
0.1	0.3	2.48	4.85	5.00	4.27	4.46
0.1	0.37	3.16	7.37	7.58	7.30	7.01
0.2	0.3	2.30	4.52	4.57	5.11	4.08
0.3	0.3	1.91	3.53	3.54	3.65	3.20
0.4	0.3	1.67	2.75	2.73	2.94	2.53
0.5	0.3	1.52	2.18	2.14	2.34	2.05
0.5	0.4	1.58	2.85	2.79	3.48	2.84
0.5	0.6	1.59	3.94	3.87	5.66	4.28
1.0	0.4	1.25	1.16	1.10	1.31	1.20
1.0	0.5	1.28	1.38	1.32	1.67	1.53
1.0	0.6	1.29	1.62	1.50	2.31	1.86
1.0	0.8	1.30	2.03	1.84	2.99	2.49
1.7	0.6	1.15	0.72	0.73	0.87	0.82
1.7	0.8	1.16	0.91	0.89	1.20	1.10
1.7	1.2	1.17	1.25	1.16	1.88	1.67
3.0	0.8	1.08	0.37	0.40	0.44	0.42
3.0	1.2	1.09	0.50	0.55	0.73	0.63
3.0	1.8	1.10	0.68	0.73	0.98	0.95
6.0	3.0	1.05	0.31	0.39	0.48	0.45
20.0	6.0	1.01	0.06	0.09	0.07	0.09

perature, the radial distribution function is given by Eq. (4.22), where $f_0(r)$ is provided by Eq. (4.10) and $f_n(r)$ with $n \geq 1$ are the inverse Laplace transforms of the functions (4.8). Some needed specific values are given by Eqs. (4.11), (4.12), and (4.18). The parameters L_1, S_1, S_2, and S_3 are linear functions of L_0, as shown by Eqs. (4.2)–(4.5), and the latter quantity is the solution of Eq. (4.21). Finally, the polynomial $Q(r)$ is given by Eq. (4.23), where the explicit expressions for the coefficients A, B, and C can be found in Eqs. (4.25), (4.28), and (4.29), the two latter supplemented by Eqs. (4.30) and (4.31), where $y(1)$ is given by Eq. (4.20). All the expressions are analytical, except Eq. (4.21),which must be solved numerically to obtain L_0 for given η and x. Note that, in order to determine $g(r)$ for $r < k =$ integer, where in practice $k=3$ is enough, only the functions $f_n(r)$ with $n \leq k-1$ are needed. They can be explicitly obtained by application of the residue theorem, as illustrated in Eq. (4.10) for $n=0$. Alternatively, one can use any of the efficient methods discussed by Abate and Whitt [39] to numerically invert Laplace transforms.

The LT theory for PSs proposed in this section is within the spirit of the rational-function approximation that has been applied in the past to hard-core systems [38]. In fact, as indicated before, it is straightforward to prove that the LT $g(r)$ given by Eq. (4.22) reduces to the PY $g(r)$ in the HS limit $(x \to 1 \Rightarrow L_0 \to 1)$. The HS limit of the LT $y(r)$ for $r < 1$ is presented in Appendix C. It turns out that the resulting function, Eq. (C5), gives values that are practically indistinguishable from those obtained for HSs by Eqs. (3.17) and

(3.18) implemented with Eq. (3.21). It is also be proven in Appendix C that our LT approximation (4.22) for PSs is consistent with the exact form (2.3) of $y(r)$ to first order in density.

V. THE HIGH-TEMPERATURE (HT) APPROXIMATION

The exact asymptotic behavior (2.6) in the limit $T^* \to \infty$ can be used to propose a simple approximation that might be useful for high temperatures, in the same spirit as done in the 1D case [29]. The key point of the approximation is the assumption that the cavity function $y(r)$ depends on the distance r and the state variables x and η only through the combination $xw(r)$, where $w(r)$ is the inverse Fourier transform of Eq. (2.7), which depends on x and η through the product ηx. This general assumption can be formally expressed as

$$y(r) = \mathcal{F}(xw(r)), \qquad (5.1)$$

where the function $\mathcal{F}(z)$ remains to be chosen. Consistency with Eq. (2.6) imposes the constraint

$$\mathcal{F}(z) = 1 + z + \mathcal{O}(z^2). \qquad (5.2)$$

We have found that $\mathcal{F}(z) = 1 + z e^z$ compares with MC simulations for high temperatures better than other simple possibilities, such as $\mathcal{F}(z) = 1 + z$, $\mathcal{F}(z) = e^z$, or $\mathcal{F}(z) = (1 - z)^{-1}$. Therefore the high-temperature (HT) approximation adopted in this paper is

$$y(r) = 1 + xw(r) e^{xw(r)}. \qquad (5.3)$$

We have also checked that Eq. (5.3) is superior to the mean-field approximation $c(r) = f(r)$, where $c(r)$ is the direct correlation function and $f(r) = -x\Theta(1 - r)$ is the Mayer function. The Ornstein-Zernike relation then yields $g(r) = 1 + xw(r) + f(r)$, which implies

$$y(r) = 1 + xw(r)\left[1 + \frac{x}{1 - x}\Theta(1 - r)\right]. \qquad (5.4)$$

While the mean-field approximation (5.4) is also consistent with the exact behavior (2.6), it does not belong in the class of approximations (5.1). In fact, all the approximations of the form (5.1) satisfying Eq. (5.2) are consistent with the exact low-density behavior (2.3), while the mean-field approximation (5.4) is not.

VI. COMPARISON WITH MC SIMULATIONS

Here we compare our two heuristic theories with MC simulations and with the results obtained by the numerical solution of two classical integral equation theories: the PY and the HNC approximations.

We first fix the packing fraction at $\eta = 0.3$ and increase the temperature from $T^* = 0.1$ to $T^* = 0.5$. The results for $g(r)$ are shown in Fig. 3. We observe that the LT, PY, and HNC theories practically coincide with the simulation results outside the core $(r > 1)$, while the HT approximation does it for longer distances $(r \gtrsim 2)$. In any case, the interesting region
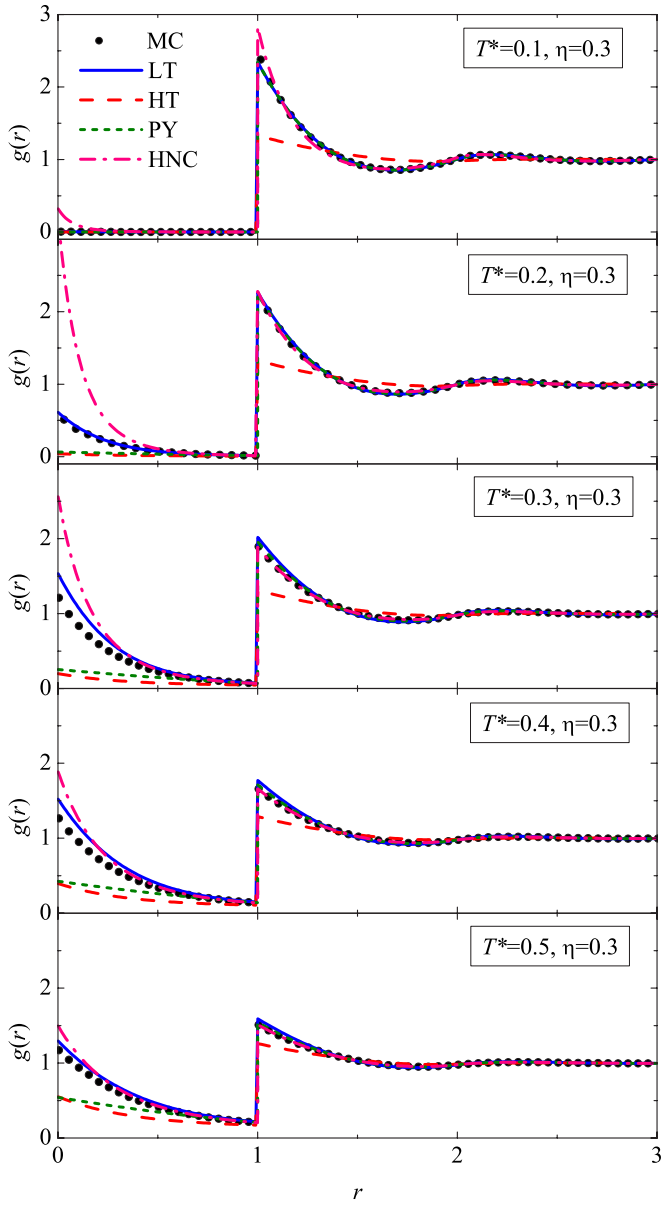
FIG. 3. (Color online) Plot of the radial distribution function at $\eta=0.3$ and for temperatures $T^*=0.1$, $T^*=0.2$, $T^*=0.3$, $T^*=0.4$, and $T^*=0.5$. The circles are MC simulation data, while the lines correspond to the LT approximation (—), the HT approximation (– – –), the PY theory (- - -), and the HNC theory (–·–).

for the PS model is the overlapping one ($0 \leq r \leq 1$) and it is there where the largest discrepancies appear. As expected from the behavior of $y(r)$ in the zero-temperature limit (see Fig. 2) and also for low densities [30], the PY theory strongly underestimates $g(r)$ in the overlapping region. We will see in subsequent figures that this drawback persists for higher densities and/or temperatures. As for the HNC theory, it tends to overestimate $g(r)$ for $r<1$, this effect being dramatic at very low temperatures (say $T^*=0.1$ and $T^*=0.2$) but rapidly diminishing its importance as the temperature increases. In fact, the HNC theory performs a remarkable good job at $T^*=0.4$ and $T^*=0.5$, except near the origin. Concerning the HT approximation, it is not surprising that it is so poor, given the range of temperatures considered in Fig. 3. The most noticeable feature is that our LT approximation, which only re-
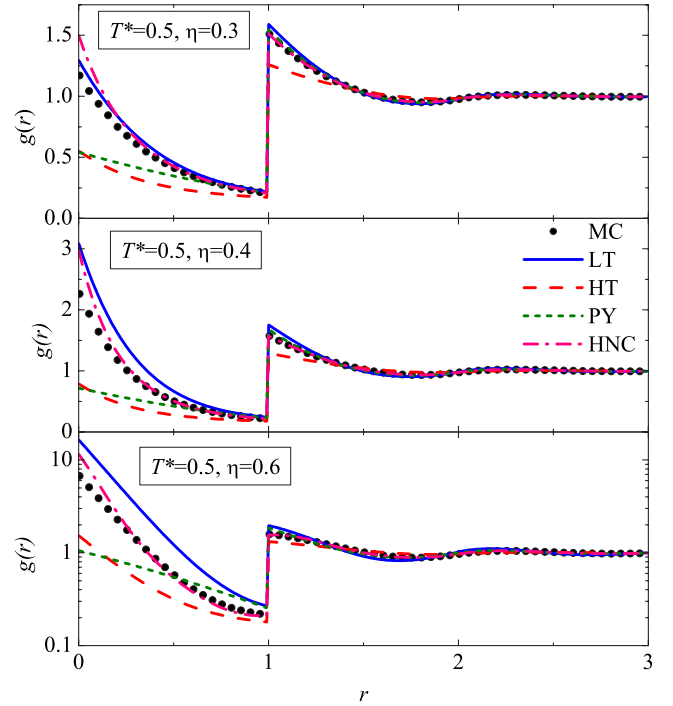

FIG. 4. (Color online) Plot of the radial distribution function at $T^*=0.5$ and for densities $\eta=0.3$, $\eta=0.4$, and $\eta=0.6$. The circles are MC simulation data, while the lines correspond to the LT approximation (—), the HT approximation (– – –), the PY theory (- - -), and the HNC theory (–·–).

quires to solve numerically Eq. (4.21), exhibits a surprisingly good agreement with simulation for the states considered. Therefore it achieves its goal of extending to low temperatures the good role played in the case of HSs by the (modified) PY theory described in Sec. III. While the temperature $T^*=0.1$ ($1-x \simeq 5 \times 10^{-5}$) is so low that the PS fluid with a packing fraction $\eta=0.3$ behaves practically as the HS system, and so $g(r) \approx 0$ for $r<1$, for temperatures larger than $T^*=0.2$ ($1-x \approx 7 \times 10^{-3}$) the number of overlapped pairs becomes observable. The state $\eta=0.3$ and $T^*=0.2$ was already considered in Refs. [19,21], where it was also found that the PY and HNC theories were highly insufficient in that case.

In Figs. 4–7 we consider the temperatures $T^*=0.5$, $T^*=1$, $T^*=1.7$, and $T^*=3$, respectively, and several increasing densities in each case. The values of the densities are chosen as to make the product ηx (which is the relevant parameter in the high-temperature limit [26]) ranging from $\eta x \simeq 0.25$ to $\eta x \simeq 0.5$. The 17 independent states considered in Figs. 3–7 are represented in Fig. 8.

It is observed in Figs. 4–7 that the HNC theory provides excellent predictions for $T^* \geq 0.5$ at any density. In contrast, as anticipated before, the PY theory keeps being very limited at short distances, although it tends to improve as the temperature increases. With respect to the LT approach, Figs. 4–7 confirm that it starts failing as the temperature grows. The density also plays an important role since, at a given temperature, the quality of the LT predictions worsens with increasing density. In any case, it is remarkable that the LT theory is rather good for temperatures as high as $T^*=1.7$,
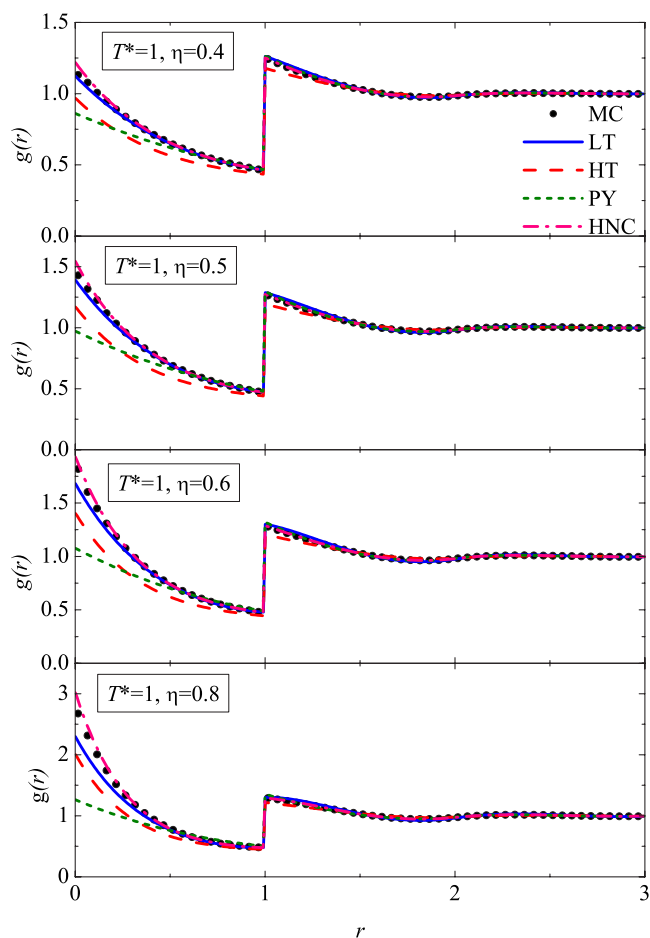
FIG. 5. (Color online) Plot of the radial distribution function at $T^*=1$ and for densities $\eta=0.4$, $\eta=0.5$, $\eta=0.6$, and $\eta=0.8$. The circles are MC simulation data, while the lines correspond to the LT approximation (—), the HT approximation (– – –), the PY theory (- - -), and the HNC theory (—·—).

provided that the density is not large (say $\eta \lesssim 0.6$). However, the LT theory visibly deteriorates for higher temperatures and densities, developing an artificial local minimum at a distance $r<1$. In contrast, the HT theory, as expected, becomes more accurate when the temperature and the density increase. In fact at $T^*=3$ the HT curves practically coincide with the HNC ones.

As shown in Figs. 3–7, the LT and HT theories complement each other: the former becomes more accurate as the temperature and/or the density decrease, while the opposite happens for the HT theory. In fact, both heuristic theories meet and become practically equivalent at certain intermediate temperatures and densities, as illustrated by the top panel of Fig. 6. In order to characterize the "basins of attraction" of each theory in the density-temperature plane, let us define the locus of state points where the contact quantity $y(1)$ $=g(1^+)$ takes the same value in both approximations. This locus, which is plotted in Fig. 8, separates the basins of each approximation. As one departs from this curve, the quality of the corresponding approximation (either LT or HT) significantly improves, as illustrated by Fig. 3 in the LT case and by Fig. 7 in the HT case. Figure 8 also includes Kirkwood's
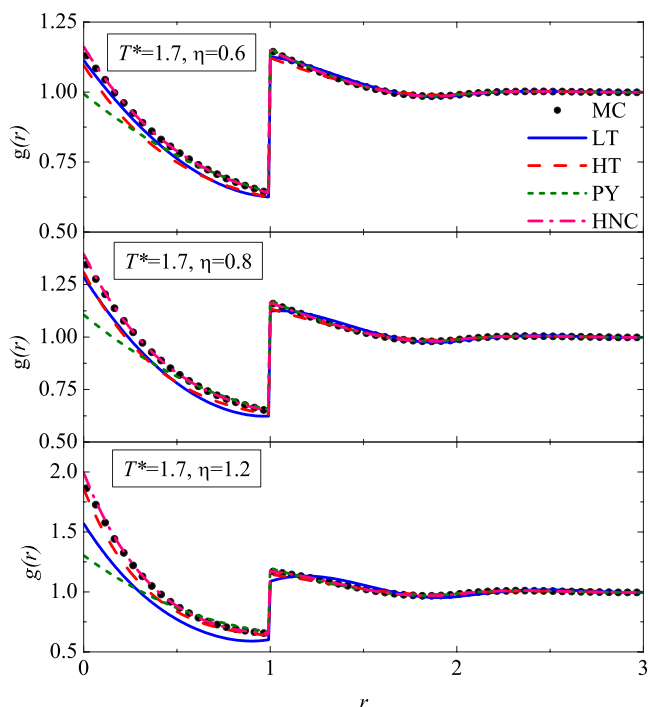

FIG. 6. (Color online) Plot of the radial distribution function at $T^*=1.7$ and for densities $\eta=0.6$, $\eta=0.8$, and $\eta=1.2$. The circles are MC simulation data, while the lines correspond to the LT approximation (—), the HT approximation (– – –), the PY theory (- - -), and the HNC theory (—·—).

instability line $\eta x=1.45$, above which the function $w(r)$ is not defined. In the high-temperature limit the freezing transition has been estimated to occur at $\eta x \simeq 0.6$ [26]. The extrapolation of this value to any temperature provides an (admittedly rough) estimate of the freezing curve (dashed-dotted line in Fig. 8). Therefore the fluid is stable approximately below that curve and it is in that region where the domains of the LT and HT approximations are meaningful.

VII. SUMMARY AND CONCLUDING REMARKS

In this paper we have investigated the structural properties of the PS model by computational, numerical, and analytical tools. In the limit of asymptotically high temperatures the linear chain diagrams contributing to the virial expansion of the cavity function dominate, their sum giving rise to Eqs. (2.6) and (2.7). The auxiliary function $w(r)$ depends on density and temperature only through the scaled quantity ηx, where x is defined by Eq. (2.2), and its series expansion converges uniformly for $\eta x < \frac{1}{8}$.

In the opposite zero-temperature limit, the system becomes an HS fluid, whose expression for $g(r)$ in the PY approximation is known exactly in Laplace space. Since the particles are impenetrable in this limit, $g(r)$ vanishes for $r <1$. However, the cavity function $y(r)$ remains different from zero, its determination being important to understand the behavior of $g(r)$ for low (but nonzero) temperatures, as shown in Fig. 1. We have seen that the cavity function for $r<1$ predicted by the PY theory for HSs is extremely poor
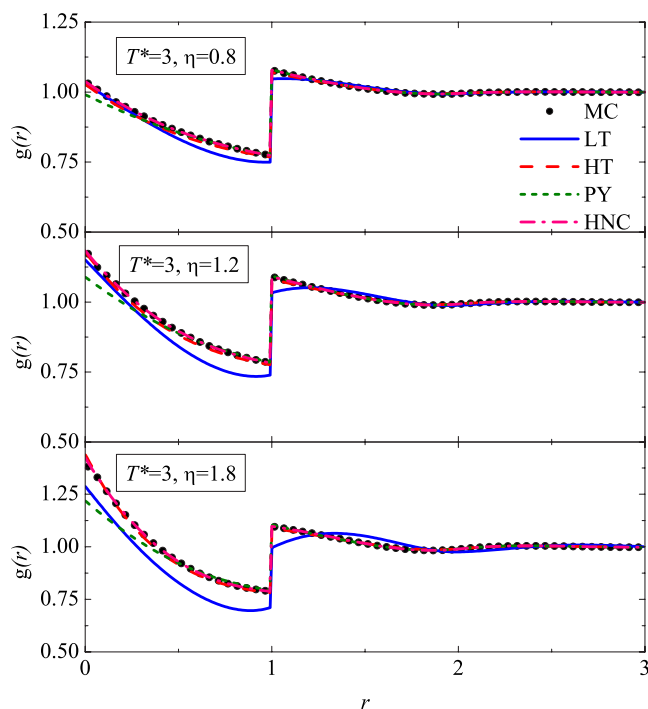
FIG. 7. (Color online) Plot of the radial distribution function at $T^*=3$ and for densities $\eta=0.8$, $\eta=1.2$, and $\eta=1.8$. The circles are MC simulation data, while the lines correspond to the LT approximation (—), the HT approximation (– – –), the PY theory (- - -), and the HNC theory (−·−).

(cf. Fig. 2), this effect being a precursor of the tendency of the PY theory to dramatically underestimate the penetrability phenomenon at finite temperatures. However, the modified
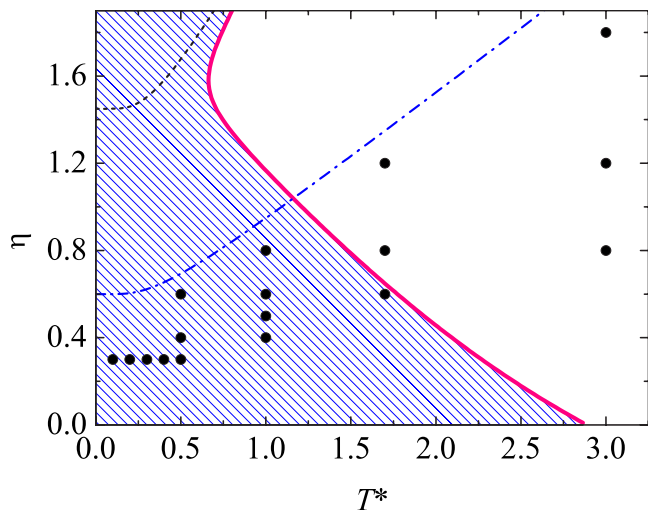

FIG. 8. (Color online) The circles represent the states considered in Figs. 3–7. The thick solid line represents the locus of points where the LT and HT approximations predict the same value of the contact quantity $y(1)=g(1^+)$. The LT approximation is more accurate in the shaded region to the left of the curve, while the HT approximation is more accurate to the right of the curve. The dashed-dotted line is a rough estimate of the freezing curve, while the dashed line represents the threshold curve (Kirkwood's instability line) above which the HT theory ceases to exist.

version (3.17), implemented with the consistent zero-separation values (3.15) and (3.16), represents a significant improvement. Slightly better results are obtained when Eq. (3.15) is replaced by Eq. (3.21).

Based on the explicit expression of $g(r)$ obtained from the PY approximation in the HS limit, complemented by Eq. (3.17), we have proposed an approximate theory which, by construction, should be accurate for very low temperatures (LT). This LT approximation is given by Eq. (4.22), where the Laplace transforms of the functions $f_n(r)$ can be found in Eqs. (4.7) and (4.8) and the polynomial $Q(r)$ is given by Eq. (4.23). The coefficients appearing in those functions are determined by imposing consistency conditions, namely the physical requirement (A3), the continuity of $y(r)$ and $y'(r)$ at $r=1$, and prescribed expressions for the zero-separation values $y(0)$ and $y'(0)$. For the latter two quantities we have proposed approximate extensions to finite temperatures of the zero-separation theorems holding in the case of HSs. Those extensions, which are given by Eqs. (4.30) and (4.31), are reasonably accurate for wide ranges of temperature and density, as shown in Table I. All the coefficients are explicitly expressed in terms of one of them (chosen to be L_0), which is obtained as the solution of a closed transcendental equation, Eq. (4.21), stemming from the continuity condition $y(1^-)=y(1^+)$.

The LT theory has been complemented by a simpler approximation constructed by exploiting the exact asymptotic behavior of the correlation functions for high temperatures. Among several possibilities, we have taken Eq. (5.3) as our high-temperature (HT) approximation, which agrees with simulation results better than the mean-field approximation (5.4).

In order to test the LT and HT theories from moderately low to moderately high temperatures, we have carried out MC simulations for the 17 states represented in Fig. 8. We have also numerically solved the PY and HNC integral equations for each one of those states. The results show that the LT theory is the best one for $T^* \leq 0.4$ and does a very good job for higher temperatures, provided the density is not too large. It is a reasonable approximation even at a temperature $T^*=1.7$ and a density $\eta=0.6$. However, it rapidly deteriorates for higher temperatures (for instance, at $T^*=3$). As the LT approximation worsens, the HT theory improves and becomes very accurate for $T^* \geq 1.7$. Figure 8 shows the regions in the parameter space η–T^* where each theory is expected to be more reliable.

Regarding the classical integral equation theories, we have found that the HNC approximation is excellent, except for low temperatures ($T^* \leq 0.4$), its performance increasing with temperature. This is similar to the situation in 1D [29] and agrees with recent results obtained for the generalized exponential model with $n=4$ [6]. On the other hand, the PY theory is generally very poor near $r=0$, especially for low temperatures.

The importance of having analytical treatments for the structural properties of fluids at one's disposal cannot be overemphasized. From that point of view, we believe that the LT and HT theories constructed here can be useful to describe the spatial correlation functions of the PS model with-

out the burden of numerically solving integral equations. Both theories complement each other and thus their combined use covers satisfactorily well the whole range of densities and temperatures. Of course, it would be desirable to have a unique *analytical* approximation equally accurate for both low and high temperatures. However, this does not seem to be an easy task at all. As a matter of fact, the PS model represents an interesting benchmark for liquid theory since it encompasses different regimes: the HS system at very low temperatures and finite densities, the ideal gas at very high temperatures and finite densities, and the mean-field system at very high temperatures and densities.

APPENDIX A: LAPLACE TRANSFORM

The Laplace transform of $rg(r)$ is defined as

$$G(t) = \int_0^\infty dr\, e^{-rt} r g(r). \qquad (A1)$$

The relationship between $G(t)$ and the Laplace transform $H(t)$ of $rh(r)$, where $h(r)=g(r)-1$ is the total correlation function, is

$$G(t) = \frac{1}{t^2} + H(t). \qquad (A2)$$

The isothermal compressibility is directly related to $dH(t)/dt|_{t=0}$ and is finite. Therefore $H(t)$ must be finite at $t=0$, so that the small-t behavior of $G(t)$ must be

$$G(t) = \frac{1}{t^2}[1 + \mathcal{O}(t^2)]. \qquad (A3)$$

The large-t behavior of $G(t)$ is also easy to find. Near the origin, Eq. (2.1) implies that $g(r) = (1-x)[y(0) + y'(0)r + \mathcal{O}(r^2)]$, so that

$$G(t) = \frac{1-x}{t^2}[y(0) + 2y'(0)t^{-1} + \mathcal{O}(t^{-2})]. \qquad (A4)$$

Now we define an auxiliary function $P(t)$ by

$$G(t) = \frac{t}{12\eta} \frac{P(t)}{1 + P(t)}. \qquad (A5)$$

Thus Eqs. (A3) and (A4) are equivalent to

$$P(t) = -1 - \frac{1}{12\eta} t^3 + \mathcal{O}(t^5), \qquad (A6)$$

$$P(t) = 12\eta \frac{1-x}{t^3}[y(0) + 2y'(0)t^{-1} + \mathcal{O}(t^{-2})], \qquad (A7)$$

respectively.

APPENDIX B: VIRIAL EXPANSION OF THE FUNCTION $w(r)$

The inverse Fourier transform of $\widetilde{w}(k)$ is

$$w(r) = \frac{1}{2\pi^2 r} \int_0^\infty dk\, k \sin(kr) \widetilde{w}(k). \qquad (B1)$$

Note now that Eq. (2.7) can be rewritten as

$$\widetilde{w}(k) = \frac{\pi}{6\eta x} \frac{\widetilde{F}^2(k)}{1 - \widetilde{F}(k)} = \frac{\pi}{6\eta x} \sum_{n=2}^\infty \widetilde{F}^n(k), \qquad (B2)$$

where we have called

$$\widetilde{F}(k) \equiv 24\eta x \frac{k\cos k - \sin k}{k^3}. \qquad (B3)$$

Therefore Eq. (B1) becomes

$$w(r) = \sum_{n=2}^\infty (\eta x)^{n-1} w_n(r) \qquad (B4)$$

with

$$w_n(r) = \frac{24^n}{12\pi r} \int_0^\infty dk\, k \sin(kr) \left(\frac{k\cos k - \sin k}{k^3} \right)^n. \qquad (B5)$$

Application of the residue theorem gives, after some standard but lengthy manipulations, the result

$$w_n(r) = \frac{1}{r} \sum_{m=0}^{[(n-1)/2]} (n - 2m - r)^{2(n-1)} \mathcal{P}_n^{(m)}(r) \Theta(n - 2m - r). \qquad (B6)$$

Here, $[k]$ denotes the integer part of k and $\mathcal{P}_n^{(m)}(r)$ is the polynomial of degree n given by

$$\mathcal{P}_n^{(m)}(r) = \sum_{p=0}^n c_{np}^{(m)} (n - 2m - r)^{n-p}, \qquad (B7)$$

with the coefficients

$$c_{np}^{(m)} = (-1)^m \frac{12^{n-1} n!}{(3n-2)!} \binom{3n-2}{p} \sum_{q=0}^p \binom{p}{q}$$

$$\times \frac{(-1)^q}{(m-p+q)!\,(n-m-q)!}. \qquad (B8)$$

From Eq. (B6) it is possible to check the relationship

$$\frac{w_n(1)}{n} + \frac{w_{n+1}(0)}{8(n+1)} = 0, \quad n \geq 2, \tag{B9}$$

which allows one to prove the thermodynamic consistency between the virial and energy routes to the equation of state [26]. The first few functions $w_n(r)$ are

$$w_2(r) = \frac{1}{2}(r-2)^2(r+4)\Theta(2-r), \tag{B10}$$

$$w_3(r) = \frac{3(r-1)^4}{35r}(r^3+4r^2-53r-162)\Theta(1-r)$$
$$- \frac{(r-3)^4}{35r}(r^3+12r^2+27r-6)\Theta(3-r), \tag{B11}$$

$$w_4(r) = -\frac{(r-2)^6}{525r}(r^4+12r^3-96r^2-1232r-2304)\Theta(2-r)$$
$$+ \frac{(r-4)^6}{2100r}(r^4+24r^3+156r^2+224r-144)\Theta(4-r). \tag{B12}$$

The series (B4) converges for $\eta x < \frac{1}{8}$ because $\widetilde{w}(k)$ is singular at $k=0$ when ηx takes the negative value $\eta x = -\frac{1}{8}$. By an adequate reordering of terms, Eq. (B4) can be rewritten as

$$w(r) = -\Theta(1-r) + r^{-1}\sum_{n=1}^{\infty}\Theta(n-r)$$
$$\times \sum_{m=0}^{\infty}[\eta x(n-r)^2]^{n+2m-1}\mathcal{P}_{n+2m}^{(m)}(r). \tag{B13}$$

Therefore $w(r)$ has a fourth-order discontinuity at $r=1$ and a discontinuity of order $2(n-1)$ at $r=n\geq 2$. For instance,

$$w''''(1^+) - w''''(1^-) = 432(\eta x)^2, \tag{B14}$$

$$w''(2^+) - w''(2^-) = -6\eta x, \tag{B15}$$

$$w''''(3^+) - w''''(3^-) = 48(\eta x)^2. \tag{B16}$$

APPENDIX C: SOME CONSEQUENCES OF THE LT THEORY

1. Zero-temperature limit of the cavity function inside the core

According to Eq. (4.24), the cavity function inside the core is

$$y(r) = (1-x)^{-1}\frac{f_0(r)}{r}e^{Q(r)}. \tag{C1}$$

Now we will take the limit $\epsilon \equiv 1-x = e^{-1/T^*} \to 0$. Let us first write $L_0 = 1 - K\epsilon + \mathcal{O}(\epsilon^2)$. Thus Eq. (4.10) becomes $f_0(r) \to K\epsilon\bar{f}_0(r)$, where

$$\bar{f}_0(r) = -\frac{1}{12\eta}\sum_{i=1}^{3}\frac{z_i e^{z_i r}}{S_1+2S_2 z_i + 3S_3 z_i^2}, \tag{C2}$$

the parameters L_1, S_1, S_2, and S_3 being now given by Eqs. (3.4)–(3.7). Near the origin, following steps similar to those of Eq. (4.14), one obtains

$$\bar{f}_0(r) = \frac{1+2\eta}{(1-\eta)^2}r\left[1 - \frac{3\eta}{1-\eta}r + \frac{3\eta^2}{(1-\eta)^2}r^2\right] + \mathcal{O}(r^4). \tag{C3}$$

According to Eq. (4.21), the coefficient K is explicitly given by

$$K = \frac{y_{\mathrm{PY}}(1)}{\bar{f}_0(1)}. \tag{C4}$$

Therefore Eq. (C1) becomes

$$y(r) = K\frac{\bar{f}_0(r)}{r}e^{Q(r)}, \tag{C5}$$

where the coefficients A, B, and C of the polynomial $Q(r)$ reduce to [cf. Eqs. (4.23), (4.25), and (4.28)–(4.31)]

$$A = 1 + \frac{y'_{\mathrm{PY}}(1)}{y_{\mathrm{PY}}(1)} - \frac{\bar{f}'_0(1)}{\bar{f}_0(1)}, \tag{C6}$$

$$B = \frac{1}{2}A + \frac{1}{2}\ln\left[\frac{y_{\mathrm{mPY}}(0)(1-\eta)^2}{(1+2\eta)K}\right], \tag{C7}$$

$$C = \frac{y'_{\mathrm{mPY}}(0)}{y_{\mathrm{mPY}}(0)} - A + 3B + \frac{3\eta}{1-\eta}. \tag{C8}$$

2. Low-density limit

To first order in density, the parameter L_0 has the form $L_0 = L_{00} + L_{01}\eta + \mathcal{O}(\eta^2)$. The coefficients L_{00} and L_{01} are determined by expanding $F_0(t)$ and $F_1(t)$ to first order in η and imposing the condition $y(1^-) = y(1^+)$ to that order. This yields, after some algebra,

$$L_0 = x + \frac{1}{2}\eta x(1-x)(3-5x) + \mathcal{O}(\eta^2). \tag{C9}$$

The functions $f_0(r)$ and $f_1(r)$ are given by

$$f_0(r) = (1-x)r\left[1 + \frac{1}{2}\eta x(5+5x-6r+r^3) + \mathcal{O}(\eta^2)\right], \tag{C10}$$

$$f_0(r) + f_1(r-1) = r\left[1 + \frac{1}{2}\eta x^2(r-2)^2(r+4) + \mathcal{O}(\eta^2)\right].$$
(C11)

Finally, use of Eqs. (4.25), (4.28), and (4.29) gives

$$A = \frac{3}{2}\eta x(1-3x) + \mathcal{O}(\eta^2), \tag{C12}$$

$$B = -\frac{1}{2}\eta x(1-x) + \mathcal{O}(\eta^2), \quad C = \mathcal{O}(\eta^2) \tag{C13}$$

It is then straightforward to check that Eq. (4.22) reduces to Eq. (2.3).

[1] M. S. Wertheim, Phys. Rev. Lett. **10**, 321 (1963); E. Thiele, J. Chem. Phys. **39**, 474 (1963).

[2] C. N. Likos, Phys. Rep. **348**, 267 (2001), and references therein.

[3] C. N. Likos, H. Löwen, M. Watzlawek, B. Abbas, O. Jucknischke, J. Allgaier, and D. Richter, Phys. Rev. Lett. **80**, 4450 (1998); M. Watzlawek, C. N. Likos, and H. Löwen, *ibid.* **82**, 5289 (1999).

[4] B. M. Mladek, D. Gottwald, G. Kahl, M. Neumann, and C. N. Likos, Phys. Rev. Lett. **96**, 045701 (2006); **97**, 019901(E) (2006).

[5] B. M. Mladek, M. J. Fernaud, G. Kahl, and M. Neumann, Condens. Matter Phys. **8**, 135 (2005).

[6] C. N. Likos, B. M. Mladek, D. Gottwald, and G. Kahl, J. Chem. Phys. **126**, 224502 (2007).

[7] F. H. Stillinger and D. K. Stillinger, Physica A **244**, 358 (1997).

[8] H. Graf and H. Löwen, Phys. Rev. E **57**, 5744 (1998).

[9] A. Lang, C. N. Likos, M. Watzlawek, and H. Löwen, J. Phys.: Condens. Matter **12**, 5087 (2000).

[10] A. A. Louis, P. G. Bolhuis, and J.-P. Hansen, Phys. Rev. E **62**, 7961 (2000).

[11] C. N. Likos, A. Lang, M. Watzlawek, and H. Löwen, Phys. Rev. E **63**, 031206 (2001).

[12] R. Finken, J.-P. Hansen, and A. A. Louis, J. Stat. Phys. **110**, 1015 (2003).

[13] B. M. Mladek, G. Kahl, and M. Neumann, J. Chem. Phys. **124**, 064503 (2006).

[14] S. Prestipino, F. Saija, and P. V. Giaquinta, Phys. Rev. E **71**, 050102(R) (2005); J. Chem. Phys. **123**, 144110 (2005); P. V. Giaquinta and F. Saija, ChemPhysChem **6**, 1768 (2005); F. Saija, S. Prestipino, and P. V. Giaquinta, J. Chem. Phys. **124**, 244504 (2006).

[15] K. Hiroike, J. Phys. Soc. Jpn. **12**, 326 (1957).

[16] L. Groome, J. W. Dufty, and M. J. Lindenfeld, Phys. Rev. A **19**, 304 (1979).

[17] C. Marquest and T. A. Witten, J. Phys. (France) **50**, 1267 (1989).

[18] W. Klein, H. Gould, R. A. Ramos, I. Clejan, and A. I. Mel'cuk, Physica A **205**, 738 (1994).

[19] C. N. Likos, M. Watzlawek, and H. Löwen, Phys. Rev. E **58**, 3135 (1998).

[20] M. Schmidt, J. Phys.: Condens. Matter **11**, 10163 (1999).

[21] M. J. Fernaud, E. Lomba, and L. L. Lee, J. Chem. Phys. **112**, 810 (2000).

[22] Y. Rosenfeld, M. Schmidt, M. Watzlawek, and H. Löwen, Phys. Rev. E **62**, 5006 (2000).

[23] M. Schmidt and M. Fuchs, J. Chem. Phys. **117**, 6308 (2002).

[24] S.-C. Kim and S.-Y. Suh, J. Chem. Phys. **117**, 9880 (2002).

[25] N. Choudhury and S. K. Ghosh, J. Chem. Phys. **119**, 4827 (2003).

[26] L. Acedo and A. Santos, Phys. Lett. A **323**, 427 (2004).

[27] A. Santos, in *Rarefied Gas Dynamics: 24th International Symposium on Rarefied Gas Dynamics*, edited by M. Capitelli, AIP Conf. Proc. No. 762 (AIP, Melville, NY, 2005), pp. 276–281.

[28] A. Santos, Mol. Phys. **104**, 3411 (2006).

[29] Al. Malijevský and A. Santos, J. Chem. Phys. **124**, 074508 (2006).

[30] A. Santos and Al. Malijevský, Phys. Rev. E **75**, 021201 (2007); **75**, 049901(E) (2007).

[31] S. Labík and A. Malijevský, Mol. Phys. **53**, 381 (1984).

[32] J. A. Cuesta and A. Sánchez, J. Phys. A **35**, 2373 (2002); J. Stat. Phys. **115**, 869 (2004).

[33] R. Balescu, *Equilibrium and Nonequilibrium Statistical Mechanics* (Wiley, New York, 1974).

[34] J.-P. Hansen and I. R. McDonald, *Theory of Simple Liquids*, 3rd. ed. (Academic Press, London, 2006).

[35] L. L. Lee, J. Chem. Phys. **103**, 9388 (1995); L. L. Lee, D. Ghonasgi, and E. Lomba, *ibid.* **104**, 8058 (1996); L. L. Lee and A. Malijevský, *ibid.* **114**, 7109 (2001).

[36] In the MC simulations presented in this paper we have employed the conventional Metropolis algorithm on an NVT ensemble with periodic boundary conditions. Typically, $N = 10^4$ particles are used. In each realization, the correlation functions are measured every 100 MC sweeps and this cycle is repeated 2×10^4 times. The time-averaged quantities are further averaged over ten independent realizations.

[37] S. B. Yuste and A. Santos, Phys. Rev. A **43**, 5418 (1991).

[38] M. López de Haro, S. B. Yuste, and A. Santos, in *Playing with Marbles: Theory and Simulation of Hard-Sphere Fluids and Related Systems*, edited by A. Mulero (Springer, in press); e-print arXiv:0704.0157 [cond-mat.stat-mech].

[39] J. Abate and W. Whitt, Queueing Syst. **10**, 5 (1992).